VIP Nanotubes

DOI: 10.1002/anie.200900546

# Bismuth-Catalyzed Growth of $SnS_2$ Nanotubes and Their Stability**

*Aswani Yella, Enrico Mugnaioli, Martin Panthöfer, Helen Annal Therese, Ute Kolb, and Wolfgang Tremel**

*Dedicated to Professor Reinhard Nesper on the occasion of his 60th birthday*

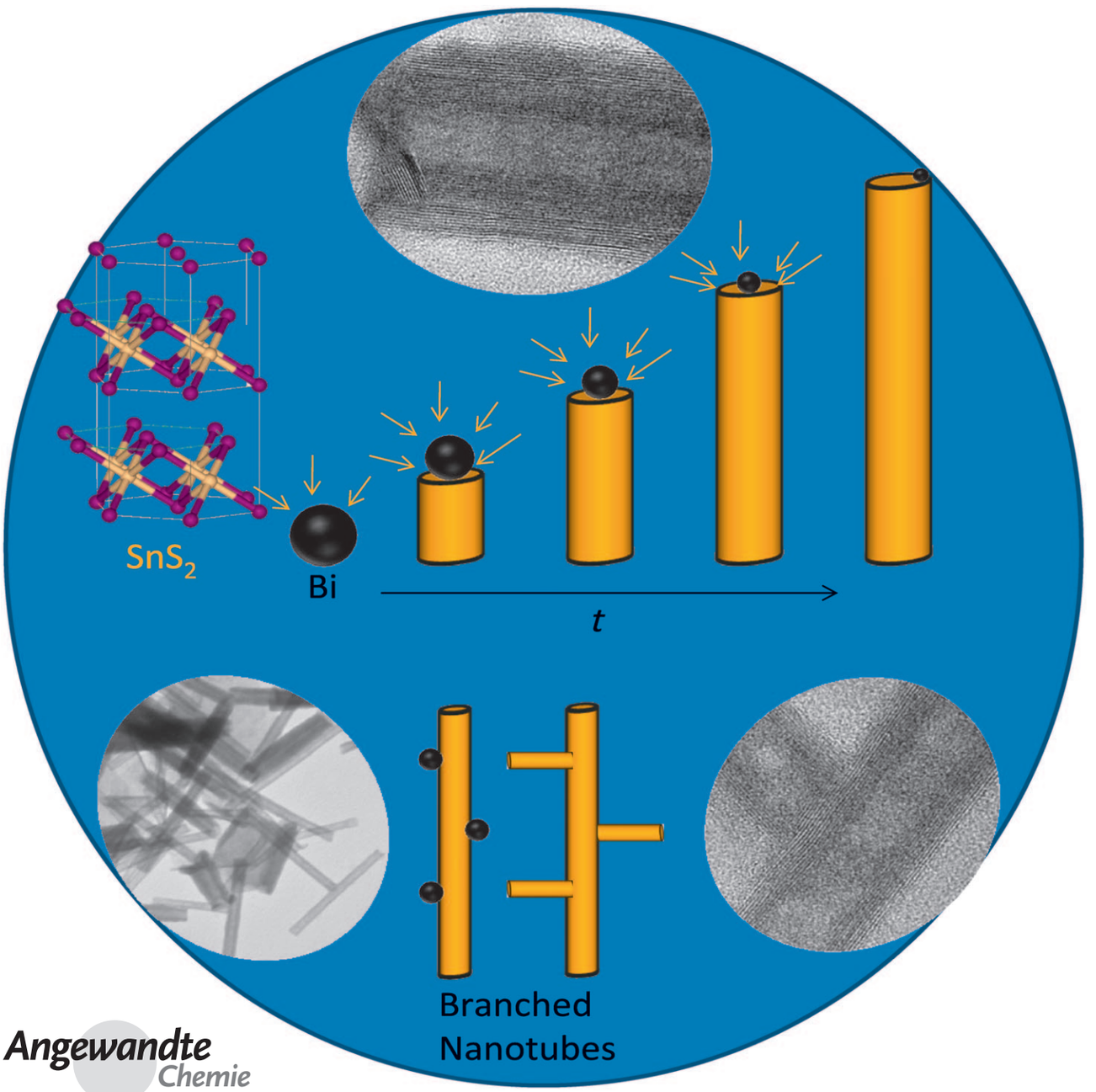

Along with carbon nanotubes, non-carbon nanostructures have attracted much attention over the past few years. Owing to their unusual geometry and promising physical properties, the study of inorganic fullerene nanostructures has become one of the key topics in nanoscale research since the first report on $WS_2$ nanotubes by Tenne et al. in 1992.[1] Various approaches to other nanotubes, such as $NiCl_2$,[2] $VS_2$,[3] $TiS_2$,[4] and InS[5] have also been reported, which implies many substances with layered structures may form nanotubes under favorable conditions. However, the synthesis of chalcogenide nanotubes and chalcogenide fullerenes (inorganic fullerenes, IF) is, in contrast to carbon, difficult owing to their wall thickness of three atom layers; considerable strain energy is required to achieve surface curvature.[6] Layered chalcogenides ($MQ_2$, M = Mo, W, Re, or Sn) are namely triple-layer structures in which one metal layer is sandwiched between two chalcogenide layers.[7] Furthermore, the formation of curved $MQ_2$ morphologies commonly involves a considerable number of lattice defects and dislocations.[8] Since the first observation of single nanotubes,[1] significant progress has been made, and today gram quantities of some metal chalcogenide nanotubes can be obtained in pure form. The two most efficient synthetic approaches are the reductive sulfidization of oxide films[9] or particles[10] and the template deposition in porous alumina.[11] Other synthetic approaches make use of the direct pyrolysis of artificial lamellar mesostructures,[12] sonoelectrochemical bath reactions,[13] and electron-beam irradiation in the electron transmission microscope.[14]

A particular problem in the synthesis of nanotubes and fullerene-type nanoparticles is that they are high-temperature and low-pressure phases. High preparation temperatures are needed to interconnect the edges of single-layer fragments through the formation of point defects, which provide curvature to the otherwise flat slabs. The instable reaction intermediates have to be trapped before they can polymerize in follow-up reactions; a similar concept was successful in matrix isolation spectroscopy. In practice, dilution at low pressure prevents the formation of larger aggregates in the gas phase. In fact, most successful strategies for the formation of nanotubes and fullerene-type species rely on gas-phase reactions, in which the reactive gas-phase species are trapped by "shock freezing". In the case of tin disulfide, the decomposition temperature is however far lower than the temperature required to interconnect the edges of single-layer fragments.

Our approach to tin disulfide nanotube growth (Figure 1) exploits recent developments in metal-catalyzed nanowire synthesis, in which monodisperse metal nanodroplets are used to form Group 13/15 and Group 14 semiconductor nanowires

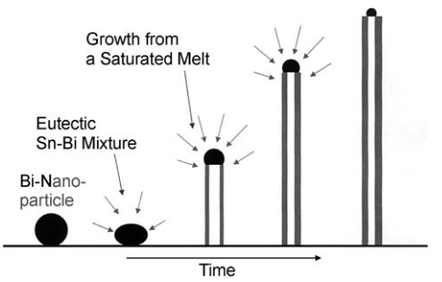


***Figure 1.*** Proposed growth mechanism of the $SnS_2$ nanotubes with a bismuth catalyst.

through a vapor–liquid–solid (VLS) growth process.[17] The diameter[15] and the length[16] of the nanowires are controlled by the size of the nearly monodisperse metal clusters and the growth time, respectively.[17] The vapor-phase semiconductor reactants required for nanowire growth are formed by heating solid $SnS_2$ nanoflakes, and an inert carrier gas provides the required dilution of the vapor-phase species. The metal droplets catalyze the formation of nanotubes by providing a nucleation surface. This approach can be successfully implemented if a catalyst suitable for the growth of the metal chalcogenide can be identified. Previous studies[18] suggest that bismuth nanoclusters meet this requirement for some metal chalcogenides.

Herein we report on the synthesis of $SnS_2$ nanotubes starting from nanometer-sized $SnS_2$ flakes using bismuth metal droplets as a catalyst. Bulk tin disulfide, $SnS_2$, adopts the layered $CdI_2$ structure that is based on a hexagonal closest-packed anion that stacks with every second layer of octahedral sites occupied by cations.[19] The low interlayer interaction energy allows the formation of stacking variants, and many polytype structures of $SnS_2$ have been described.[20] The thermodynamically stable polytype of $SnS_2$ at ambient conditions is the trigonal modification ($P\bar{3}m1$, $a = 3.6486$ Å, $c = 5.8992$ Å). Recently Tenne and co-workers obtained closed-cage fullerene-like (IF) nanoparticles of tin sulfide by laser ablation.[21] However, these fullerenes are not pure tin disulfide, but rather contain superstructures created by a periodic stacking of layered $SnS_2$ and SnS that are reminiscent of the misfit compounds $AMS_3$ (A = Sn, Pb, Sb, Bi, M = Ti, V, Cr, Nb, Ta).[22]

We obtained $SnS_2$ nanotubes (NT-$SnS_2$) in a two-step process: In the first step, $SnS_2$ nanoflakes were prepared by heating aqueous solutions of $SnCl_4 \cdot 5H_2O$ and HCl with thioacetamide for 12 h in a teflon-lined autoclave at 120 °C. After cooling, the solid residue was collected by filtration and

[*] A. Yella, Dr. M. Panthöfer, Dr. H. A. Therese, Prof. Dr. W. Tremel
Institut für Anorganische Chemie und Analytische Chemie der
Johannes Gutenberg-Universität
Duesbergweg 10–14, 55099 Mainz (Germany)
Fax: (+49) 6131-39-25605
E-mail: tremel@uni-mainz.de
Dr. E. Mugnaioli, Dr. U. Kolb
Institut für Physikalische Chemie der
Johannes Gutenberg-Universität
Welderweg 11, 55099 Mainz (Germany)

[**] We thank G. Glasser and Dr. M. N. Tahir for SEM measurements. This research was supported by a fellowship to A.Y. from POLYMAT, the Graduate School of Excellence of the State of Rhineland-Palatinate. We are indebted for support from the Materials Science Center (MWFZ) in Mainz and the DFG within the priority program 1165 "Nanotubes and Nanowires: From Controlled Synthesis to Function".

Supporting information for this article is available on the WWW under http://dx.doi.org/10.1002/anie.200900546.

  

dried. In the second step, the $SnS_2$ nanoflakes were transformed to $SnS_2$ nanotubes (NT-$SnS_2$) by the catalytic action of bismuth droplets. The high yield of $SnS_2$ nanotubes allowed us to perform various analyses, including X-ray diffraction (XRD) and X-ray fluorescence (RFA).

Figure 2a shows a powder X-ray diffraction pattern of the $SnS_2$ precursor product obtained from the first reaction step. The broad reflections indicate small crystallite sizes. A TEM image (Supporting Information, Figure S1) reveals that the $SnS_2$ precursor product contains nanoflakes with diameters of

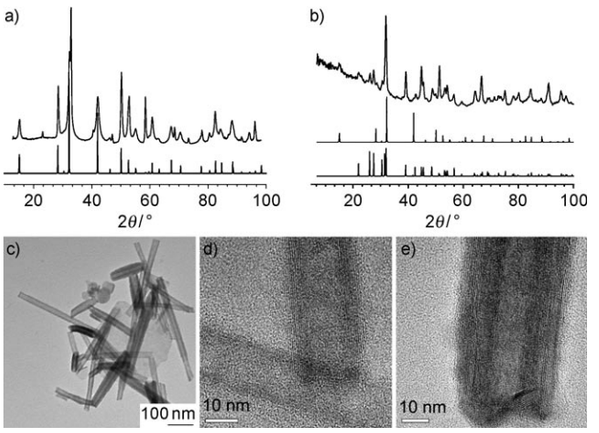


***Figure 2.*** a) Powder X-ray diffraction pattern (top) of $SnS_2$ nanoflakes. The bottom line corresponds to the calculated diffractogram of $SnS_2$ (Berndtite 2T). b) Powder X-ray diffraction pattern of NT-$SnS_2$ (top) and calculated line powder patterns of $SnS_2$-4H (middle, PDF-2 no.21-1231) and SnS (bottom, PDF-2 no.39-0354). c) TEM image of the obtained product. HRTEM images of d) an open-ended nanotube and e) a closed-end nanotube.

10–30 nm. These nanoflakes were used as starting material for the synthesis of the $SnS_2$ nanotubes. In the second step of the reaction, the $SnS_2$ nanoflakes were mixed with bismuth powder, and the product was obtained at the colder end of the tube furnace after the heat treatment in a stream of argon. A typical X-ray powder diffraction pattern of the product is shown in Figure 2b, which shows that the product mainly consists of $SnS_2$-4H, with some amount of SnS.

Figure 2c shows a TEM image of the product. It consists of almost pure one-dimensional nanotubes with diameters ranging from 30 to 40 nm. The lengths of the nanotubes are typically between 100 and 500 nm. The aspect ratio of the nanowires was estimated to be about 5–50, which is much lower than the typical range for $WS_2$ nanotubes (> 200).[9,10] High-resolution transmission electron microscopy (HRTEM) images of the $SnS_2$ nanotubes (Figure 2d,e) show clearly the multiwalled structure. The interlayer spacing is about 0.60 nm, which corresponds to the (001) lattice planes of $SnS_2$.

The growth of semiconductor nanowires by laser ablation has been reported.[15] In these experiments, a metallic seed particle (usually gold) acts as catalyst in that it acts as the location where the reactant is preferentially adsorbed. In the experiments,[15] gold nanoclusters were supported on a $SiO_2$ substrate, and the gas-phase concentration of the reactants was increased by laser pulses. The alloy droplets remain as spheres at the end of the wire, and are driven forward by the growth front. Therefore, the nanowires are grown at low temperature where the growth on the uncatalyzed side surfaces is kinetically hindered. The unidirectional growth is usually explained by the vapor–liquid–solid (VLS) mechanism, by which a liquid droplet works as a preferential sink for the growth elements that precipitate at the liquid–gas phase boundary.

As bismuth and tin are known to form a eutectic mixture at about 150 °C, we reasoned that bismuth droplets might act as a sink for the growth species ($SnS_2$ and/or sulfur) from the gas phase, and subsequently as a seed for the growth of the $SnS_2$ nanotubes. The $SnS_2$ nanotubes might therefore have a low defect density owing to the low reaction temperatures and thus low deviation from the ideal stoichiometry (1:2) and the resulting formation of SnS:$SnS_2$ intergrowth structures. In fact, the as-synthesized $SnS_2$ nanotubes were very crystalline: The walls are composed of regularly ordered $SnS_2$ layers and have a low density of defects, such as stacking faults or missing layers.

Some of the nanotubes were found to contain bismuth droplets at their tips (Figure 3). A representative HRTEM image of single-component nanotube (Figure 3a) shows that the reaction produces straight $SnS_2$ nanotubes, and a bismuth droplet is attached to one end. The diameters of the $SnS_2$ nanotubes range from 10 to 50 nm, depending on the thickness of the evaporated bismuth droplet, and their lengths vary from 100 to 500 nm. Unfortunately, under the 200 keV electron beam, the bismuth droplets disappear within 30 s, leaving behind only the $SnS_2$ nanotube. A similar observation was made during the synthesis of branched PbSe nanowires.[23] energy dispersive X-ray spectroscopy (EDX) was used to examine the local elemental composition of the $SnS_2$ nanotubes (Figure 3c). The composition of the nanotube at the tip

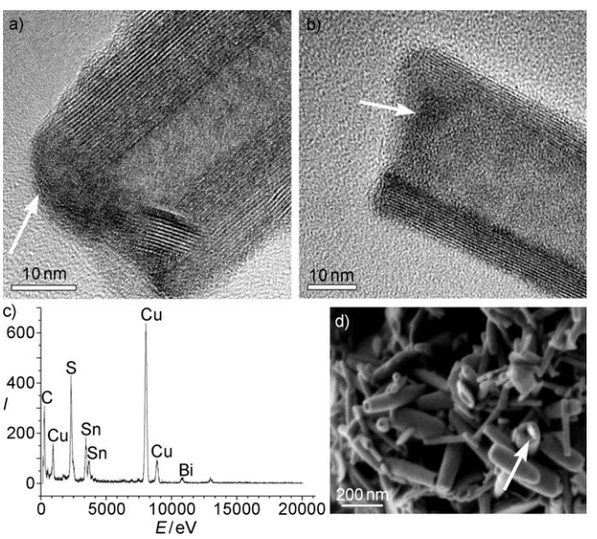


***Figure 3.*** a,b) HRTEM images showing the tips of $SnS_2$ nanotubes. Arrows indicate traces of bismuth droplets present at the end the nanotubes. c) EDX spectrum of the area indicated in (a). d) SEM image of nanotube heterostructures. The arrow indicates traces of bismuth droplets present at the end of a nanotube.

  

yields a (Sn,Bi):S atomic ratio of 1:2, with up to 3% of bismuth content.

To identify the effect of the bismuth catalyst, control experiments were also carried out in the absence of bismuth, again using $SnS_2$ nanoflakes as the starting material. In these experiments, no nanotubes were produced; micro-sized crystallites and amorphous materials appeared to be the main products (see Supporting Information, Figure S1). These results clearly indicate that the bismuth catalyst is essential for the growth of the $SnS_2$ nanotubes.

As the temperature for the transformation of the $SnS_2$ nanoflakes to nanotubes is significantly higher than the melting/decomposition temperature of the crystalline tin disulfide, experiments with crystalline tin disulfide ($SnS_2$) and crystalline tin sulphide (SnS) were carried out to determine whether $SnS_2$ nanoflakes are a necessary precursor for the formation of $SnS_2$ nanotubes. In the case of crystalline tin disulfide, the nanotubes had similar dimensions as the nanotubes obtained with $SnS_2$ nanoflakes; when crystalline SnS was used, the nanotubes were smaller than those obtained with tin disulfide (see Figure 4). The formation of smaller nanotubes with SnS as precursor might result from a lower sulfur vapor pressure.

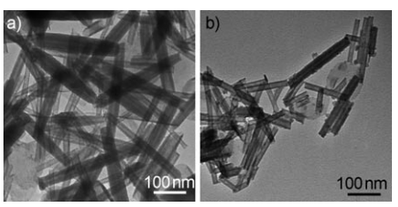


***Figure 4.*** TEM images of nanotubes obtained when bulk $SnS_2$ (a) and bulk SnS (b) were used as precursors for the synthesis of $SnS_2$ nanotubes.

An important phenomenon of the VLS growth is the appearance of metal catalyst particles at the tips of nanotubes. However, for the majority of the $SnS_2$, nanotubes no bismuth droplets could be detected. We believe that the absence of catalyst nanoparticles on the nanotube tips after synthesis might be due to the shrinkage and disappearance of catalysts through evaporation owing to the high vapor pressure of bismuth. Another possible mechanism is through diffusion, which has recently been suggested in tapered silicon nanowires grown using gold nanoparticles as catalysts.[24]

Even though bismuth tips were not found on the edges of the nanotubes, some branched, T-shaped nanotubes were present (Figure 5a). Figure 5b shows the high-resolution TEM image of a branched nanotube. In this sense, the branching growth displayed here is an in situ analogue of the previously demonstrated branched nanowire growth of Group 13/15 semiconductors using intentionally added VLS metal catalysts with other materials systems,[25] and it is also related to InAs nanowire formation with continuous feeding of a manganese catalyst.[26]

The diameter of the nanowire in VLS growth is usually determined by the size of the catalyst particle. As these particles are generated in situ during the reaction, their size cannot be controlled, which leads to the formation of catalyst

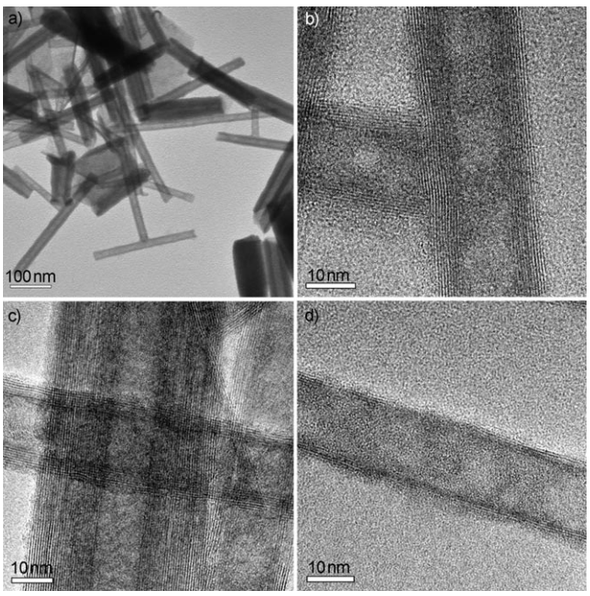


***Figure 5.*** a) TEM and b) HRTEM images of branched nanotubes, which confirm the growth of the nanotubes by VLS growth from bismuth nanoparticle. c,d) HRTEM images of nanotubes with different diameters: c) Nanotubes with diameters of 40 nm and 15 nm; d) single nanotube with a diameter of 10 nm.

particles with different sizes. This in turn results in the formation of nanotubes with different diameters (Figure 5).

As sulfur is known to permeate from the metal sulfides (in particular under the conditions of laser ablation),[21] and $SnS_2$ can form superlattices with SnS as reported earlier,[21] $SnS_2$ nanotubes were annealed under argon by slow heating

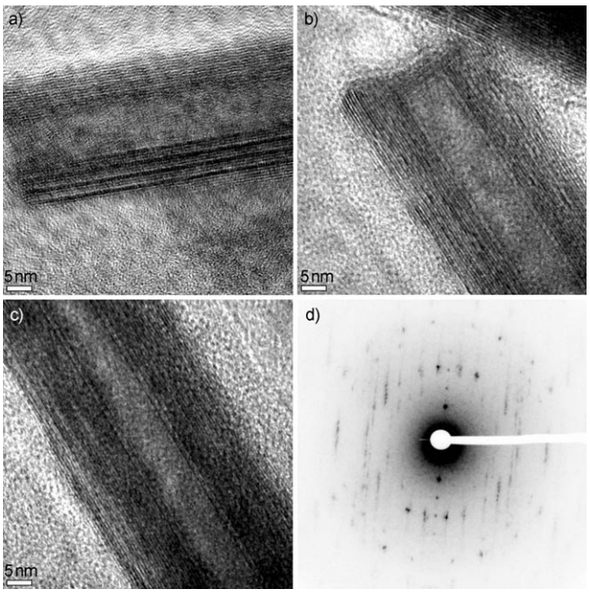


***Figure 6.*** HRTEM images of $SnS_2$ nanotubes annealed for 1 h at 300 °C. a) Tip of an open nanotube, b) tip of a closed nanotube, c) middle of a nanotube, d) electron diffraction pattern of a $SnS_2$ nanotube.

  

(2 °C min$^{-1}$) and kept at 300 °C for 1 hr (Figure 6). After annealing, some agglomeration of the nanotubes was observed, and some of the nanotubes were deformed. From the HRTEM images, $SnS_2$/SnS superlattices were formed, and the electron diffraction pattern indicated a doubling of the interlayer distance to 1.2 nm.

In summary, $SnS_2$ nanotubes have been synthesized by a transformation of layered $SnS_2$ sheets to $SnS_2$ nanotubes through the catalytic action of bismuth nanodroplets. The development of approaches for a controlled growth of nanocrystalline heterostructures may significantly expand the range of applications of nanocrystals. The ease of fabrication of large amounts of nanocrystalline heterostructures by simple high-temperature methods fulfills an important requirement for their use as building blocks in nanotechnology. A nanotube with a single nanodroplet attached to one end may for example act as a preferential anchoring point for substrates of a magnetic material, or as a "navigation" sensor in magnetic fields.

## Experimental Section

The preparation of $SnS_2$ nanotubes was carried out in a quartz tube (inside diameter 2 cm) that was placed in a horizontal tube furnace. $SnS_2$ nanoflakes, prepared from $SnCl_4 \cdot 5H_2O$ and thioacetamide, and bismuth powder (in molar ratio 5:1) were loaded in a corundum boat (trade name: Degussit) and initially kept at one end of a horizontal tube furnace. The tube furnace was purged with high-purity argon (Ar 4.6) for 1 h prior to heating to remove any oxygen in the furnace. The furnace was then heated to 800 °C at a rate of 5 °C min$^{-1}$. The corundum boat was moved from the edge to the middle of the furnace, where the temperature was 800 °C, under the flow of argon and kept at this temperature for 2 h; argon acted both as protecting medium and carrier gas. During the heating process, the argon flow rate was kept at 200 sccm (standard cubic centimeters per minute). Argon was run after the heating process until the furnace is cooled to room temperature to avoid oxidation of the prepared sulfide products. The products were formed at the upper side of the tube in the low-temperature zone (due to the natural temperature gradient, $T = 200$–$250$ °C) of the furnace. The sample was subsequently collected from the tube (colder tube end for those samples heated in a temperature gradient).

The resulting samples from both steps were examined by XRD (Bruker AXS D8 microdiffractometer, Cu $K_{\alpha 1}$ radiation, graphite monochromator, equipped with a 2D HiStar detector), scanning electron microscopy (HRSEM, LEO 1530 field-emission SEM, 6 kV extraction voltage), transmission electron microscopy (Philips EM420, or Philips CM12, acceleration voltage 120 kV) and high-resolution transmission electron microscopy (Philips FEI TECNAI F30 ST electron microscope, field-emission gun, 300 kV extraction voltage and equipped with a ring-shaped high-angle dark-field detector, Gatan imaging filter, and a Si(Li) detector with an ultra-thin Be window for EDX).

Received: January 29, 2009
Published online: June 9, 2009

**Keywords:** chalcogenides · heterogeneous catalysis · nanotubes · tin · VLS process

[1] a) R. Tenne, L. Margulis, M. Genut, G. Hodes, *Nature* **1992**, *360*, 444–446; b) Y. Feldman, E. Wasserman, D. J. Srolovita, R. Tenne, *Science* **1995**, *267*, 222–225.

[2] Y. R. Hachohen, E. Grunbaum, J. Sloan, J. L. Hutchison, R. Tenne, *Nature* **1998**, *395*, 336–337.

[3] H. A. Therese, F. Rocker, A. Reiber, J. Li, M. Stepputat, G. Glasser, U. Kolb, W. Tremel, *Angew. Chem.* **2005**, *117*, 267–270; *Angew. Chem. Int. Ed.* **2005**, *44*, 262–265.

[4] J. Chen, S.-L. Li, Z.-L. Tao, Y.-T. Shen, C.-X. Cui, *J. Am. Chem. Soc.* **2003**, *125*, 5284–5285.

[5] J. A. Hollingsworth, D. M. Poojary, A. Clearfied, W. E. Buhro, *J. Am. Chem. Soc.* **2000**, *122*, 3562–3563.

[6] a) D. J. Srolovitz, S. A. Safran, M. Homyonfer, R. Tenne, *Phys. Rev. Lett.* **1995**, *74*, 1779–1782; b) N. G. Chopra, R. J. Luyren, K. Cherry, V. H. Crespi, M. L. Cohen, S. G. Louis, A. Zettl, *Science* **1995**, *269*, 966–967.

[7] W. Tremel, E. W. Finckh, *Chem. Unserer Zeit* **2004**, *38*, 326–339.

[8] D. Li, X. L. Li, R. R. He, J. Zhu, Z. X. Deng, *J. Am. Chem. Soc.* **2002**, *124*, 1411–1416.

[9] A. Rothschild, J. Sloan, R. Tenne, *J. Am. Chem. Soc.* **2000**, *122*, 5169–5179.

[10] H. A. Therese, J. Li, U. Kolb, W. Tremel, *Solid State Sci.* **2005**, *7*, 67–72.

[11] C. M. Zelenski, P. K. Dorhout, *J. Am. Chem. Soc.* **1998**, *120*, 734–742; G. Chen, G.-Z. Shen, K.-B. Tang, Y.-K. Liu, Y.-T. Qian, *Appl. Phys. A* **2003**, *77*, 747–749.

[12] Y. D. Li, X. L. Li, R. R. He, J. Zhu, Z. X. Deng, *J. Am. Chem. Soc.* **2002**, *124*, 1411–1416.

[13] Y. Mastai, M. Homyonfer, A. Gedanken, G. Hodes, *Adv. Mater.* **1999**, *11*, 1010–1013.

[14] M. Jose. Yacaman, H. Lopes, P. Santiago, D. H. Galvan, I. L. Garzon, A. Reyes, *Appl. Phys. Lett.* **1996**, *69*, 1065–1067.

[15] a) M. S. Gudiksen, C. M. Lieber, *J. Am. Chem. Soc.* **2000**, *122*, 8801–8802.

[16] Y. Cui, L. J. Lauhon, M. S. Gudiksen, J. F. Wang, C. M. Lieber, *Appl. Phys. Lett.* **2001**, *78*, 2214–2216.

[17] R. S. Wagner in *Whisker Technology*, Wiley-Interscience, New York, **1970**, pp. 47–119.

[18] L. Ouyang, K. N. Maher, C. L. Yu, J. McCarty, H. Park, *J. Am. Chem. Soc.* **2007**, *129*, 133–138.

[19] a) O. Madelung, U. Rössler, M. Schulz, *Landolt-Börnstein—Group III Condensed Matter Numerical Data and Functional Relationships in Science and Technology: Non-Tetrahedrally Bonded Elements and Binary Compounds I*, Springer, Berlin, **1991**; b) L. E. Conroy, K. C. Park, *Inorg. Chem.* **1968**, *7*, 459–463.

[20] F. Hulliger, *Structural Chemistry of Layer-Type Phases* (Eds.: F. A. Lévy), Reidel, Dordrecht and Boston, **1977**.

[21] S. Y. Hong, R. Popovitz-Biro, Y. Prior, R. Tenne, *J. Am. Chem. Soc.* **2003**, *125*, 10470–10474.

[22] a) G. A. Wiegers, *Prog. Solid State Chem.* **1996**, *24*, 1–139; b) A. Meerschaut, *Curr. Opin. Solid State Mater. Sci.* **1996**, *1*, 250–259; c) J. Rouxel, A. Meerschaut, G. A. Wiegers, *J. Alloys Compd.* **1995**, *229*, 144–157.

[23] J. Zhu, H. Peng, C. K. Chan, K. Jarausch, X. F. Zhang, Y. Cui, *Nano Lett.* **2007**, *7*, 1095–1099.

[24] a) J. B. Hannon, S. Kodambaka, F. M. Ross, R. M. Tromp, *Nature* **2006**, *440*, 69–71; b) L. Cao, B. Garipcan, J. S. Atchison, C. Ni, B. Nabet, J. E. Spanier, *Nano Lett.* **2006**, *6*, 1852–1857.

[25] a) D. Wang, F. Qian, C. Yang, Z. Zhong, C. M. Lieber, *Nano Lett.* **2004**, *4*, 871–874; b) K. A. Dick, K. Deppert, M. W Larsson, T. Martensson, W. Seifert, L. R. Wallenberg, L. Samuelson, *Nat. Mater.* **2004**, *3*, 380–384; c) Q. Wan, E. N. Dattoli, W. Y. Fung, W. Guo, Y. Chen, X. Pan, W. Lu, *Nano Lett.* **2006**, *6*, 2909–2915; d) R. Yang, Y.-L. Chueh, J. R. Morber, R. Snyder, L.-J. Chou, Z. L. Wang, *Nano Lett.* **2007**, *7*, 269–275.

[26] S. J. May, J.-G. Zheng, B. W. Wessels, L. J. Lauhon, *Adv. Mater.* **2005**, *17*, 598–602.

  